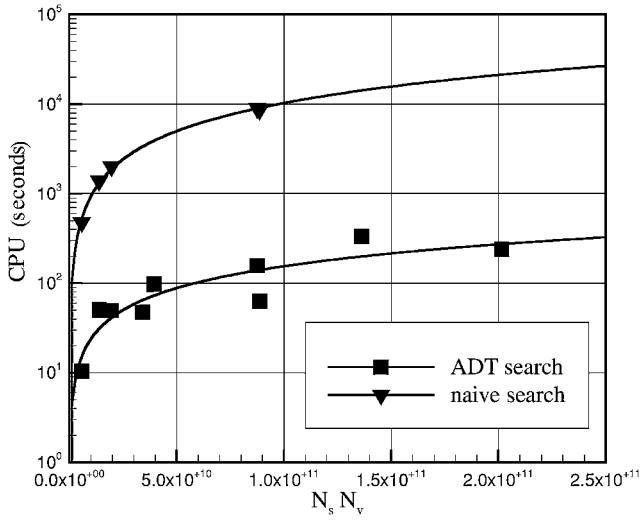

Fig. 1 Comparison of CPU time required to compute the distance from N_v points in a volume to the nearest of N_s surface points using an alternating digital tree search and a naïve search for nine internal flows.

becomes less efficient than an ordered search of the entire surface. The CPU time required by the ADT search was still lower than the naïve search but only by a factor of about four.

Conclusions

An $\mathcal{O}(N_v \log N_s)$ method for calculating wall proximity is derived by recasting the problem in a form that takes advantage of an alternating digital tree, an efficient geometric search algorithm. The method is easy to implement and is shown to reduce the CPU time by two orders of magnitude over the naive approach in the present examples.

References

[1]Baldwin, B. S., and Lomax, H., "Thin Layer Approximation and Algebraic Model for Separated Turbulent Flows," AIAA Paper 78-257, Jan. 1978.

[2]Chien, K.-Y., "Predictions of Channel and Boundary Layer Flows with a Low-Reynolds-Number Turbulence Model," *AIAA Journal*, Vol. 20, No. 1, 1982, pp. 33–38.

[3]Lai, Y. G., and So, R. M. C., "On Near-Wall Turbulent Flow Modelling," *Journal of Fluid Mechanics*, Vol. 221, 1990, pp. 641–673.

[4]Goldberg, U., Peroomian, O., and Chakravarthy, S., "A Wall-Distance-Free k–ε Model with Enhanced Near-Wall Treatment," *Journal of Fluids Engineering*, Vol. 120, No. 3, 1998, pp. 457–462.

[5]So, R. M. C., and Yuan, S. P., "A Geometry Independent Near-Wall Reynolds-Stress Closure," *International Journal of Engineering Science*, Vol. 37, No. 1, 1999, pp. 33–57.

[6]Craft, T. J., and Launder, B. E., "A Reynolds Stress Closure Designed for Complex Geometries," *International Journal of Heat and Fluid Flow*, Vol. 17, No. 3, 1996, pp. 245–254.

[7]Tucker, P. G., "Assessment of Geometric Multilevel Convergence Robustness and a Wall Distance Method for Flows with Multiple Internal Boundaries," *Applied Mathematical Modelling*, Vol. 22, No. 4–5, 1998, pp. 293–311.

[8]Tucker, P. G., "Prediction of Turbulent Oscillatory Flows in Complex Systems," *International Journal for Numerical Methods in Fluids*, Vol. 33, No. 6, 2000, pp. 869–895.

[9]Sethian, J. A., "Fast Marching Methods," *SIAM Review*, Vol. 41, No. 2, 1999, pp. 199–235.

[10]Buleev, N. I., "Theoretical Model of the Mechanism of Turbulent Exchange in Fluid Flows," Atomic Energy Research Establishment, AERE Translation 957, Harwell, England, U.K., May 1963.

[11]Launder, B. E., and Ying, W. M., "Prediction of Flow and Heat Transfer in Ducts of Square Cross-Section," *Proceedings of the Institution of Mechanical Engineers*, Vol. 187, Pt. 1, No. 37, 1973, pp. 455–461.

[12]Leslie, D. C., "Discussion of Prediction of Flow and Heat Transfer in Ducts of Square Cross-Section," *Proceedings of the Institution of Mechanical Engineers*, Vol. 187, Pt. 1, No. 37, 1973, pp. D147, D148.

[13]Gessner, F. B., and Po, J. K., "A Reynolds Stress Model for Turbulent Corner Flows, Part II: Comparisons Between Theory and Experiment," *Journal of Fluids Engineering*, Vol. 98, No. 2, 1976, pp. 269–277.

[14]Chima, R. V., and Yokota, J. W., "Numerical Analysis of Three-Dimensional Viscous Internal Flows," NASA TM 100878, July 1988.

[15]Bonet, J., and Peraire, J., "An Alternating Digital Tree (ADT) Algorithm for 3D Geometric Searching and Intersection Problems," *International Journal for Numerical Methods in Engineering*, Vol. 31, No. 1, 1991, pp. 1–17.

[16]Wang, Z. J., and Parthasarathy, V., "Fully Automated Chimera Methodology for Multiple Moving Body Problems," *International Journal for Numerical Methods in Fluids*, Vol. 33, No. 7, 2000, pp. 919–938.

R. M. C. So
Associate Editor

Improved Rhie–Chow Interpolation for Unsteady Flow Computations

Wen Zhong Shen,* Jess A. Michelsen,* and Jens Nørkær Sørensen*
Technical University of Denmark, DK-2800 Lyngby, Denmark

I. Introduction

FINITE difference and finite volume methods for solving the incompressible Navier–Stokes equations are based on either of two different grid categories: staggered grid or nonstaggered grid. Using staggered grids[1–3] typically results in stable and robust solutions.

For general nonorthogonal meshes, however, the staggered methods tend to become rather complex, either storing all velocity components on every cell face or introducing derivatives of the grid curvature through the Christoffel symbol.

To avoid these difficulties, several researchers, for example, see Ref. 4, investigated nonstaggered methods. These early schemes had no means of avoiding pressure oscillations arising from the use of 2δ differences of the pressure.

About 20 years ago, Rhie and Chow[5] proposed a procedure using a momentum-based interpolation for the cell face mass fluxes in the continuity equation that closely imitates the staggered practice by letting mass conservation be expressed in terms of mass fluxes across cell interfaces. The mass fluxes are driven by 1δ pressure differences across the faces. Hence, velocity–pressure decoupling cannot occur.

The Rhie–Chow procedure[5] gives excellent results for steady-state problems where a large local time step is used. Majumdar[6] improved the flux interpolation to avoid solution dependency on the underrelaxation parameter of the original Rhie–Chow interpolation.[5] For unsteady flow calculation, however, when using small time steps, pressure oscillations may still appear. This phenomenon was observed by Ferziger and Peric.[7] In the present paper, the origin of the pressure oscillations is analyzed, and a remedy is proposed.

II. Numerical Method

The incompressible Navier–Stokes equations are solved by a predictor–corrector method as follows.

A. Predictor Step

The momentum equations are discretized using a second-order backward differentiation scheme in time and second-order central differences in space, except for the convective terms that are discretized by the QUICK upwinding scheme. The resulting equations

Received 22 May 2001; revision received 14 August 2001; accepted for publication 17 August 2001.

*Associate Professor, Department of Mechanical Engineering, Building 403.

for each cell can be written as

$$\left(A_P + \frac{1.5J\rho}{\delta t}\right)u_P^* + \sum_{\text{EWNS}} A_i u_i^* = \frac{J\rho}{\delta t}\left(2u_P^n - 0.5u_P^{n-1}\right) - y_\eta \delta\xi\delta\eta p_\xi^n + y_\xi \delta\xi\delta\eta p_\eta^n \tag{1}$$

$$\left(A_P + \frac{1.5J\rho}{\delta t}\right)v_P^* + \sum_{\text{EWNS}} A_i v_i^* = \frac{J\rho}{\delta t}\left(2v_P^n - 0.5v_P^{n-1}\right) + x_\eta \delta\xi\delta\eta p_\xi^n - x_\xi \delta\xi\delta\eta p_\eta^n \tag{2}$$

where x and y are the Cartesian coordinates and ξ and η are curvilinear coordinates, A_P and A_i are the coefficients from the spatial discretization of convection and diffusion, and the compass summation notation

$$\sum_{\text{EWNS}}$$

is adopted. The pressure forces acting on the cell, of volume J, are tentatively evaluated at prior time t^n. Solution of Eqs. (1) and (2) yields intermediate velocity components, u^* and v^*, which do not satisfy mass conservation.

B. Corrector Step

1. Rhie–Chow Interpolation[5]

The pressure at time t^{n+1} may be expressed as a correction $p^{n+1} = p^n + p'$. Introducing the pressure correction into Eqs. (1) and (2) yields the corrected velocities

$$u^{n+1} = u^* - \left(\frac{y_\eta \delta\xi\delta\eta}{A_P^*}\right)p'_\xi + \left(\frac{y_\xi \delta\xi\delta\eta}{A_P^*}\right)p'_\eta \tag{3}$$

$$v^{n+1} = v^* + \left(\frac{x_\eta \delta\xi\delta\eta}{A_P^*}\right)p'_\xi - \left(\frac{x_\xi \delta\xi\delta\eta}{A_P^*}\right)p'_\eta \tag{4}$$

with $A_P^* = A_P + 1.5J\rho/\delta t$. For notation simplicity, an orthogonal mesh is considered.

Mass conservation is expressed in terms of mass fluxes across the cell faces e, w, n, and s:

$$G_{1e}^{n+1} - G_{1w}^{n+1} + G_{2n}^{n+1} - G_{2s}^{n+1} = 0 \tag{5}$$

where the fluxes are related to velocity as $G_1 = uy_\eta - vx_\eta$ and $G_2 = vx_\xi - uy_\xi$. The correction of cell face fluxes can now be written as

$$G_1^{n+1} = G_1^* + \overline{B/A_P^*}\,p'_\xi \qquad G_2^{n+1} = G_2^* + \overline{C/A_P^*}\,p'_\eta \tag{6}$$

where $B = -(x_\eta^2 + y_\eta^2)\delta\xi\delta\eta$, $C = -(x_\xi^2 + y_\xi^2)\delta\xi\delta\eta$, and an overbar denotes linear interpolation from cell centers to cell faces.

To compute G^*, for example G_{1e}^*, Rhie and Chow[5] proposed the interpolation

$$G_{1e}^* = \overline{F_1}|_e + \overline{B/A_P^*}\Big|_e\left(p_E^n - p_P^n\right) \tag{7}$$

introducing the auxiliary flux $F_1 = \tilde{u}y_\eta - \tilde{v}x_\eta$, based on the auxiliary velocity $(\tilde{u}, \tilde{v})$

$$\tilde{u}_P = \left[\frac{J\rho}{\delta t}\left(2u_P^n - 0.5u_P^{n-1}\right) - \sum_{\text{EWNS}} A_i u_i^*\right]\Big/ A_P^*$$

$$\tilde{v}_P = \left[\frac{J\rho}{\delta t}\left(2v_P^n - 0.5v_P^{n-1}\right) - \sum_{\text{EWNS}} A_i v_i^*\right]\Big/ A_P^* \tag{8}$$

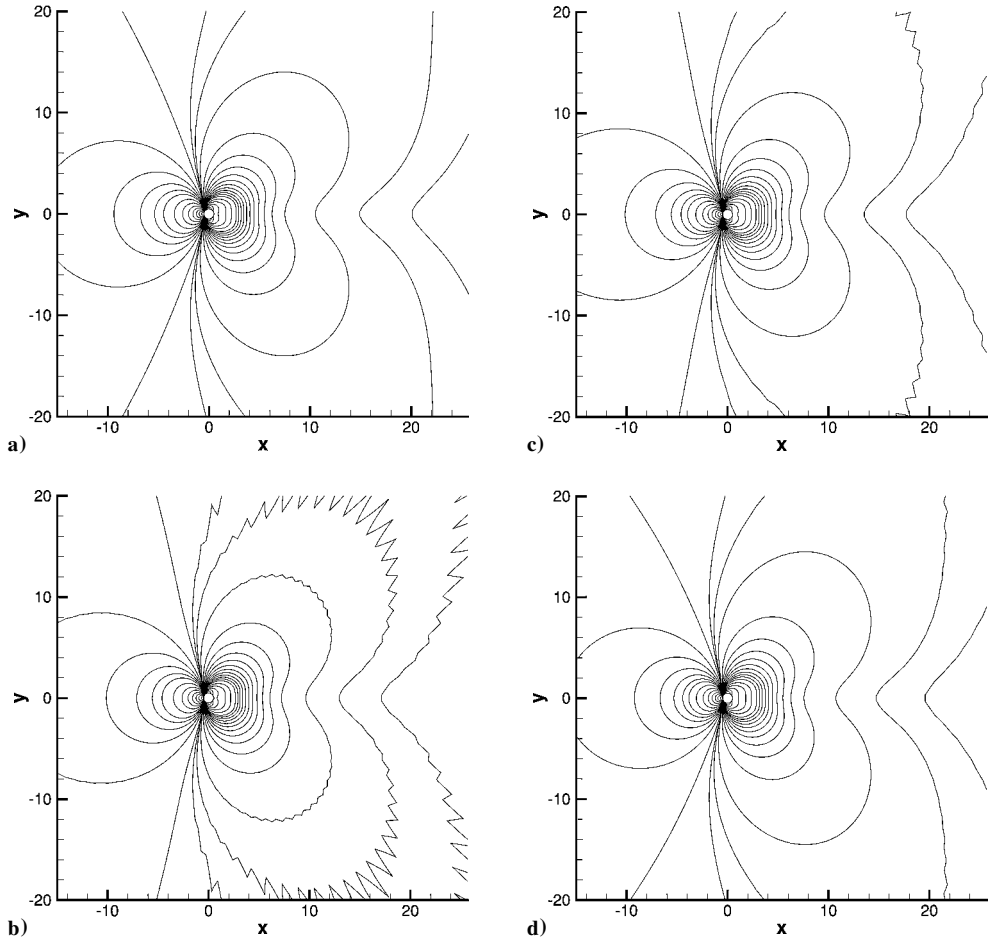

Fig. 1 Pressure contours for flows past a cylinder at $Re = 40$: a) new Rhie–Chow interpolation with $\delta t = 0.001$, b) original Rhie–Chow interpolation with $\delta t = 0.001$, c) original Rhie–Chow interpolation with $\delta t = 0.005$, and d) original Rhie–Chow interpolation with $\delta t = 0.01$.

Table 1 Deviation and oscillation of the original scheme about flows past a circular cylinder at $Re = 40$

	Deviation			Oscillation		
Time step	u	v	p	u	v	p
0.01	9.28×10^{-5}	9.90×10^{-5}	2.28×10^{-3}	4.81×10^{-6}	6.42×10^{-6}	1.81×10^{-5}
0.005	9.32×10^{-5}	9.92×10^{-5}	2.31×10^{-3}	8.76×10^{-6}	7.75×10^{-6}	4.10×10^{-5}
0.0025	9.33×10^{-5}	9.93×10^{-5}	2.35×10^{-3}	1.53×10^{-5}	1.09×10^{-5}	8.59×10^{-5}
0.001	9.36×10^{-5}	9.94×10^{-5}	2.39×10^{-3}	2.63×10^{-5}	1.70×10^{-5}	1.79×10^{-4}

2. Analysis of the Rhie–Chow Interpolation[5]

Let now $\delta t \to 0$. The auxiliary velocity $\tilde{u}$ and $\tilde{v}$ and fluxes then reduce to

$$\tilde{u}_P \to \left(4u_P^n - u_P^{n-1}\right)/3, \qquad \tilde{v}_P \to \left(4v_P^n - v_P^{n-1}\right)/3$$

$$\overline{F_1}|_e = 2\left(F_{1E}^n + F_{1P}^n\right)/3 - \left(F_{1E}^{n-1} + F_{1P}^{n-1}\right)/6$$

In general, the auxiliary fluxes $\bar{F}$ do not satisfy mass conservation. Inserting Eqs. (6) and (7) into the mass conservation [Eq. (5)] yields the Poisson equation for pressure

$$\overline{\left(B/A_P^*\right)}\Big|_e\left(p_E^{n+1} - p_P^{n+1}\right) + \overline{\left(B/A_P^*\right)}\Big|_w\left(p_W^{n+1} - p_P^{n+1}\right) + \overline{\left(C/A_P^*\right)}\Big|_n\left(p_N^{n+1} - p_P^{n+1}\right) + \overline{\left(C/A_P^*\right)}\Big|_s\left(p_S^{n+1} - p_P^{n+1}\right) = \overline{F_1}|_w - \overline{F_1}|_e + \overline{F_2}|_s - \overline{F_2}|_n \neq 0 \tag{9}$$

With $A_P^* \to 1.5J\rho/\delta t$, the coefficients are now proportional to the time step. Hence, the pressure is inversely proportional to the time step, that is, $|\nabla^2 p| \to \infty$, leading to unphysical behavior of the pressure at small time steps.

3. New Interpolation

The spurious pressure determined by Eq. (9) and observed by, among others, Ferziger and Peric,[7] originates from the linear interpolation Eq. (7) of the term involving u_P^n and u_P^{n-1}. Because the corresponding fluxes G_1^n and G_1^{n-1} are already computed in the previous time steps, the interpolation is not needed. We propose the following revision to the interpolation [Eq. (7)]:

$$G_{1e}^* = \overline{\left(\frac{2J\rho/\delta t}{A_P^*}\right)}\Bigg|_e G_{1e}^n - \overline{\left(\frac{0.5J\rho/\delta t}{A_P^*}\right)}\Bigg|_e G_{1e}^{n-1} + \overline{H_1}|_e + \overline{\left(\frac{B}{A_P^*}\right)}\Bigg|_e \left(p_E^n - p_P^n\right) \tag{10}$$

where H is the flux computed from the revised auxiliary velocity $(\hat{u}, \hat{v})$

$$\hat{u}_P = -\sum_{\text{EWNS}} \frac{A_i u_i^*}{A_P^*} \qquad \hat{v}_P = -\sum_{\text{EWNS}} \frac{A_i v_i^*}{A_P^*} \tag{11}$$

The mass defect based on the revised auxiliary velocities $\hat{u}$ and $\hat{v}$ vanishes for $\delta t \to 0$, hence making the revised interpolation consistent for all time steps. Note that the revised interpolation contributes no extra dissipation as compared to the original Rhie–Chow formulation.[5]

III. Numerical Results

To test and compare the revised scheme to the original Rhie–Chow formulation,[5] laminar flows past a circular cylinder are computed by using the finite volume/multiblock code EllipSys2D/3D.[8,9] The computational region ranges 42.5 cylinder diameters and is covered by an O-mesh consisting of 128 cells in the radial direction and 192 cells in the tangential direction. The mesh is equidistant in the tangential direction and stretched in the radial direction with a first cell height of 0.01766 cylinder diameters. The dimensionless time step is based on cylinder diameter and freestream velocity.

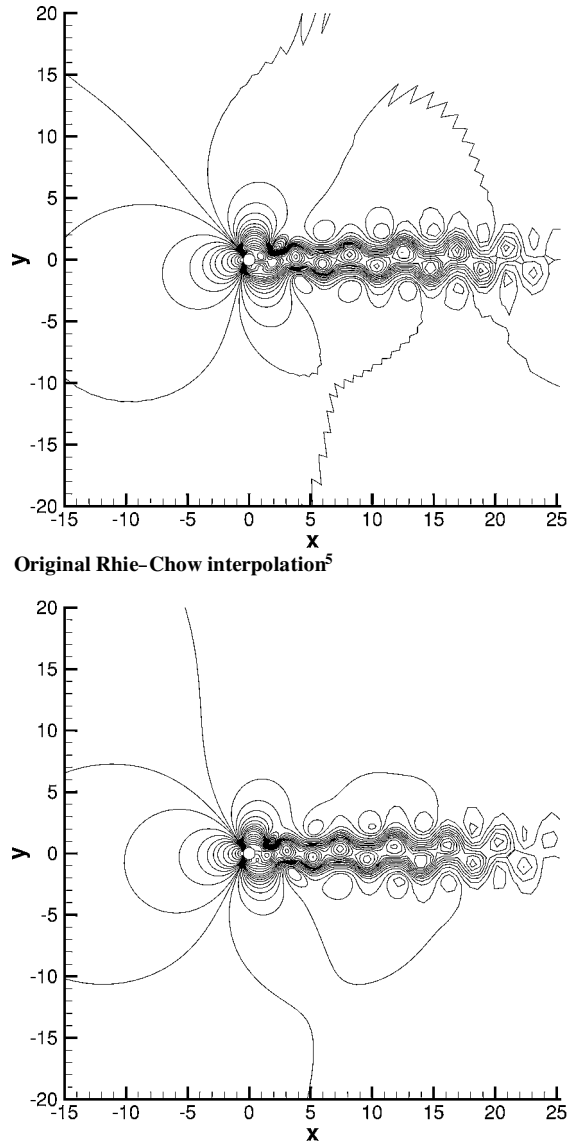

Fig. 2 Pressure contours for flows past a circular cylinder at $Re = 200$ and time step $\delta t = 0.0025$.

A. Steady-State Solution at a Reynolds Number of 40

Unsteady computations are performed at a Reynolds number of 40. At dimensionless time 500, the steady-state solution has been reached. The new interpolation gives a unique solution independent of the size of the time step.

In Fig. 1, the cell-centered pressure is plotted for different time steps. Figure 1a shows the pressure computed with the modified interpolation at a time step $\delta t = 0.001$. No oscillations can be observed. Figures 1b–1d show the pressure computed with the original

Rhie–Chow interpolation.[5] From Fig. 1, it is seen that the pressure oscillations resulting from the original Rhie–Chow interpolation are most pronounced at small time steps. To quantify the size of the deviations and oscillations, the following two quantities are computed:

$$\text{deviation} = \frac{1}{V}\int_V (s_{\text{RC}} - s_{\text{New}})\,\mathrm{d}v \tag{12}$$

$$\text{oscillation} = \frac{1}{V}\int_V \left(\delta_x^2 + \delta_y^2\right)(s_{\text{RC}} - s_{\text{New}})\,\mathrm{d}v \tag{13}$$

where s_{RC} and s_{New} are the solutions computed with the original Rhie–Chow scheme and the new scheme, respectively. The new scheme gives the same solution independent of the time step. Table 1 shows the deviation and oscillation for different time steps. From Table 1, the deviations are almost independent of the time step (from 0.01 to 0.001). The oscillations, however, become more important at decreasing time steps.

B. Unsteady Solution at a Reynolds Number of 200

The flow past a circular cylinder at Reynolds number of 200 is computed with a time step $\delta t = 0.0025$. After a dimensionless time of 200, corresponding to 80,000 time steps, a periodic solution is reached.

Figure 2 shows pressure contours computed with the modified and the original interpolation schemes. From Fig. 2, oscillations are clearly visible for the original Rhie–Chow interpolation,[5] whereas the modified interpolation displays no oscillations. For the force coefficients, the new interpolation gives almost the same values as the original interpolation scheme, except that the mean value of C_D is increased with about 0.25%.

IV. Conclusions

The origin of pressure oscillations produced by the Rhie–Chow procedure[5] when running at small time steps has been revealed. A revised procedure for the interpolation of cell face fluxes is proposed. Oscillations are succesfully eliminated by the revised procedure. The new interpolation scheme contributes no extra dissipation as compared to the Rhie–Chow procedure. The revised procedure is consistent for all time step lengths and can be used for other methods based on collocated grids, for example, the fractional step method.

References

[1]Patankar, S. V., *Numerical Heat Transfer and Fluid Flow*, Hemisphere, New York, 1980, Chap. 6.

[2]Akselvoll, K., and Moin, P., "An Efficient Method for Temporal Integration of the Navier–Stokes Equations in Confined Axisymmetric Geometries," *Journal of Computational Physics*, Vol. 125, No. 2, 1996, pp. 454–463.

[3]Karki, K. C., and Patankar, S. V., "Pressure-Based Calculation Procedure for Viscous Flows at All Speeds in Arbitrary Configurations," *AIAA Journal*, Vol. 27, 1989, pp. 1167–1174.

[4]Rubin, S. G., and Harris, J. E., "Numerical Studies of Incompressible Viscous Flow in a Driven Cavity," NASA SP-378, 1975.

[5]Rhie, C. M., and Chow, W. L., "Numerical Study of the Turbulent Flow Past an Airfoil with Trailing-Edge Separation," *AIAA Journal*, Vol. 21, No. 11, 1983, pp. 1525–1532.

[6]Majumdar, S., "Role of Underrelaxation in Momentum Interpolation for Calculation of Flow with Nonstaggered Grids," *Numerical Heat Transfer*, Vol. 13, No. 1, 1988, pp. 125–132.

[7]Ferziger, J. H., and Peric, M., *Computational Methods for Fluid Dynamics*, Springer-Verlag, Berlin, 1996, Chap. 8.

[8]Michelsen, J. A., "Basis3D—A Platform for Development of Multiblock PDE Solvers," Technical Univ. of Denmark, AFM 92-05, Lyngby, Denmark, 1992.

[9]Sørensen, N. N., "General Purpose Flow Solver Applied over Hills," Risø National Lab., RISØ-R-827-(EN), Roskilde, Denmark, 1995.

R. M. C. So
Associate Editor

Side Force on an Ogive Cylinder: Effects of Freestream Turbulence

S. C. Luo,* K. B. Lua,† and T. T. Lim*
National University of Singapore, Singapore 119260, Republic of Singapore
and
E. K. R. Goh‡
DSO National Laboratories, Singapore 118230, Republic of Singapore

Nomenclature

b	=	grid bar diameter
Cy	=	side-force coefficient, $F_y/(0.5\rho U_\infty^2 S)$
Cy_D	=	local side-force coefficient, local side force/$(0.5\rho U_\infty^2 D \sin^2\alpha)$
D	=	cylinder diameter
Fy	=	side force
I	=	turbulence intensity; I_x is the longitudinal turbulence intensity in freestream direction, σ_x/U
L	=	turbulence length scale; L_x is the longitudinal turbulence length scale in the freestream direction
M	=	mesh-opening length
P	=	pressure on model surface
P_∞	=	freestream static pressure
R	=	autocorrelation coefficient
Re_D	=	Reynolds number, $U_\infty D/\nu$
S	=	model base area, $\pi D^2/4$
T	=	timescale
U	=	time-averaged freestream velocity
X	=	axial distance from model nose tip
x	=	distance downstream from the grid
α	=	angle of attack
θ	=	azimuth angle around circular cross section measured from the most leeward position
ν	=	kinematics viscosity of fluid
ρ	=	density of fluid
σ_x	=	standard deviation of the freestream velocity
τ	=	time difference
ϕ	=	roll angle

Introduction

FREESTREAM turbulence is known to affect the side force acting on ogive cylinders pitched at high angles of attack for many years. For instance, Lamont and Hunt[1] found in their investigation that freestream turbulence caused the switching of the asymmetric flow states, resulting in a substantially smaller time-averaged side force. This finding was supported by Hunt and Dexter,[2] who conducted a study that included both high and low turbulence intensities ($I_x = 0.7$–0.01%) and found that the switching has disappeared in a "quieter" environment. In a later study Howard et al.,[3] who used four turbulence generating grids to modify freestream turbulence intensity and length scale, also found that increased turbulence intensity substantially reduced the maximum induced side force. However, not everyone seems to agree with the preceding findings. Wardlaw

Received 14 July 2000; revision received 14 December 2000; accepted for publication 19 March 2001.

*Associate Professor, Department of Mechanical Engineering, 10 Kent Ridge Crescent.
†Research Engineer, Department of Mechanical Engineering, 10 Kent Ridge Crescent.
‡Senior Member of Technical Staff, 20 Science Park Drive.